Studies on Mechanical Behavior of Glass Epoxy Composites with Induced Defects and Correlations with NDT Characterization Parameters

D. Pradeep and N. Janardhana Reddy
Department of Mechanical Engineering, VIT, Vellore

C. Rahul Kumar, L. Srikanth and R. M. V. G. K. Rao*
Fibre Reinforced Plastics Division
National Aerospace Laboratories, Bangalore – 560017, India

ABSTRACT: Degradation in mechanical properties (compression, flexural and ILS) of glass epoxy composite laminates with induced defects (simulating delaminations) was studied. The defects were characterized by using the A-scan ultrasonic pulse-echo technique. The two A-scan parameters, viz. the back wall echo amplitude and time of flight, were followed respectively, as functions of the defect size (diameter) and its location in the laminate thickness. The mechanical properties of laminates were evaluated destructively for different defect sizes and locations. An attempt has been made to express the mechanical properties in terms of the two NDT scan parameters characterizing the defects and empirical equations presented.

KEY WORDS: composites, defects, non-destructive test, ultrasonics, pulse echo, A-scan, delamination.

INTRODUCTION

One of the major limitations of composite materials is the defects that are induced during the fabrication process (e.g., voids, porosity, debonds, delaminations) and those that develop during the service life of the structure due to impact damage, that ultimately lead to reduced safety and structural performance.

According to a Boeing study in [1], about 60% of defects in composite materials that occur in aircraft components are delaminations. Therefore, reliable detection of these defects is of great importance to the quality assurance and maintenance industry. The ultrasonic pulse-echo method provides a comprehensive tool for the non-destructive evaluation of laminated composites. Posakony [2] presented experimental analysis of ultrasonic responses from artificial defects of different size and orientation, which were

*Author to whom correspondence should be addressed. E-mail: rmvgk@yahoo.com

0731-6844/07/15 1539–18 $10.00/0 DOI: 10.1177/0731684407079520

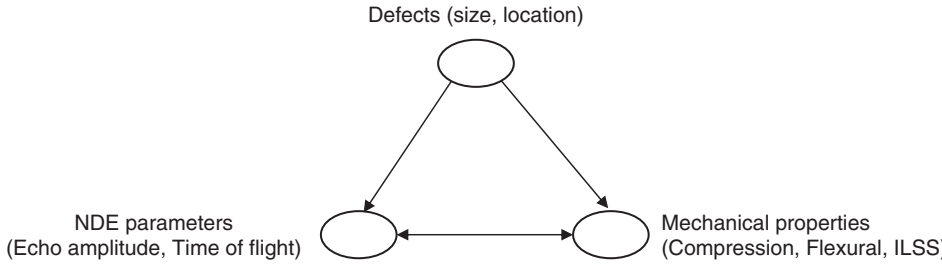

Figure 1. *Theme of the work carried out.*

machined into a 304 stainless steel flat plate. The results showed that orientation, taper of the back wall, and band width of the ultrasonic system could have significant influence on inspection results. Severin et al. [3] experimented on samples of CFRP with artificial impact damage tested by pulse-echo acoustical methods to represent the complete performance about size and position of delamination. Wooh and Wei [4] reconstructed A-scan signals for detecting delaminations caused by low velocity impacting of embedded Teflon film patches, by the ultrasonic pulse-echo technique in thin graphite/epoxy composite laminates. Bar-Cohen et al. [5] made use of amplitude and velocity measurements obtained from an ultrasonic pulse-echo technique for characterizing a variety of intrinsic defects that could come about in the manufacturing process of filament winding of glass fiber-reinforced composite tubes, through signal feature variations as a result of the anomalies encountered by ultrasonic wave in the composite structure. Judd and Wright [6] presented an interesting result indicating that the interlaminar shear strength of a composite would decrease by about 7%, for every 1% void content up to a total void content of about 4 percent.

However, not much work has been done on characterizing the delaminations in glass/epoxy laminated composites using the ultrasonic A-scan pulse-echo technique and their correlation with the properties of the composite. This paper brings out connectivity between NDE parameters, defects and strength of composite materials as shown in Figure 1, taking a standard glass-epoxy composite as candidate material, and the US A-scan as the non-destructive technique.

EXPERIMENTAL

Materials and Test Specimen Preparation

A bi-directional woven e-glass fabric (2×2 twill/280 gsm, supplied by M/s. Arun Fabrics, Bangalore) was used as the reinforcement and a bi-functional epoxy (LY 556 + HY 951, supplied by M/s. Huntsman Advanced Material (I) Pvt. Limited, India, mixed in the ratio 100:10 pbw) was the matrix used. Eight layered glass-epoxy composite laminates were fabricated with a standard vacuum bag molding technique while maintaining a constant fiber weight fraction of 0.65 ± 0.03. The laminates were RT cured for 24 h followed by post cure at 85°C for 2 h. A novel technique was used to simulate delaminations of different diameters viz. 4 mm, 6 mm and 8 mm, at various depths (at midplane, below 5th, 6th and 7th layer) by inducing a thin layer of Polyvinyl Alcohol (PVA) between the layers of glass fabric during the fabrication process (Figure 2),

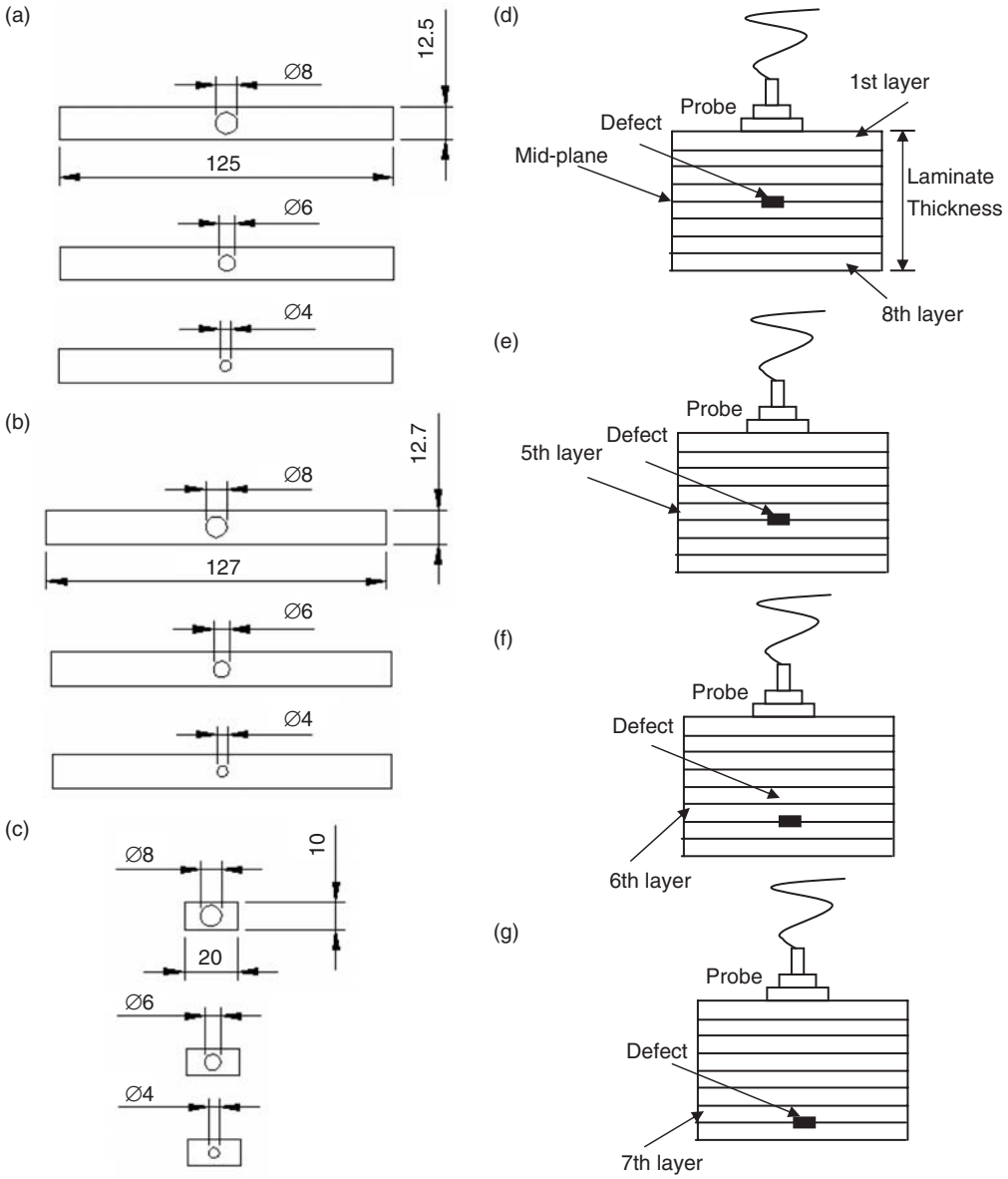

Figure 2. *Schematic showing the size and location of the induced defects. (a) Compression test specimens (b) Flexural test specimens (c) ILS test specimens (d) Defect located at midplane (below 4th layer) (e) Defect located below 5th layer (f) Defect located below 6th layer (g) Defect located below 7th layer.*

which tends to cause natural delamination upon loading. Compression, flexural and ILSS tests were conducted on specimens prepared as per ASTM standards and are shown schematically in Figure 2.

NDT CHARACTERIZATON OF DEFECTS

An ultrasonic flaw detector (Yokogawa 6200 DL model) with a pulse-echo A-scan option equipped with a 5 MHz probe was used to characterize the defects.

The pulse width of 90 ns with a gain of 20 dB and voltage of 200 V was maintained constant throughout the experiments. A schematic of the NDT technique is presented in Figure 3.

The technique consisted of positioning the specimen on a flat surface and scanning it with a probe using glycerine liquid couplant. The voltage and time base were regulated to obtain the A-scans within the 200 MHz oscilloscope screen and were recorded.

DESTRUCTIVE TESTS

Compression (ASTM D 3410), flexural (ASTM D 790) and interlaminar shear (ASTM D 2344) tests were conducted to evaluate the mechanical properties of virgin laminates as well as the laminates with induced defects, on an INSTRON 6025 model universal testing machine, maintaining a crosshead speed of 1 mm/min.

RESULTS AND DISCUSSION

Non-destructive Test Results

The A-scans of laminates with defects at various locations and of different sizes are presented in Figures 4, 5 and 6. The time of flight is represented by the distance between vertical dotted lines, indicating the depth of location of the defect from the probe (top) surface, while the back wall echo amplitude is represented by the distance between the horizontal dotted lines, indicating the size of the defect.

From Figures 4–6, the time of flight and back wall echo amplitudes measured are summarized in Table 1.

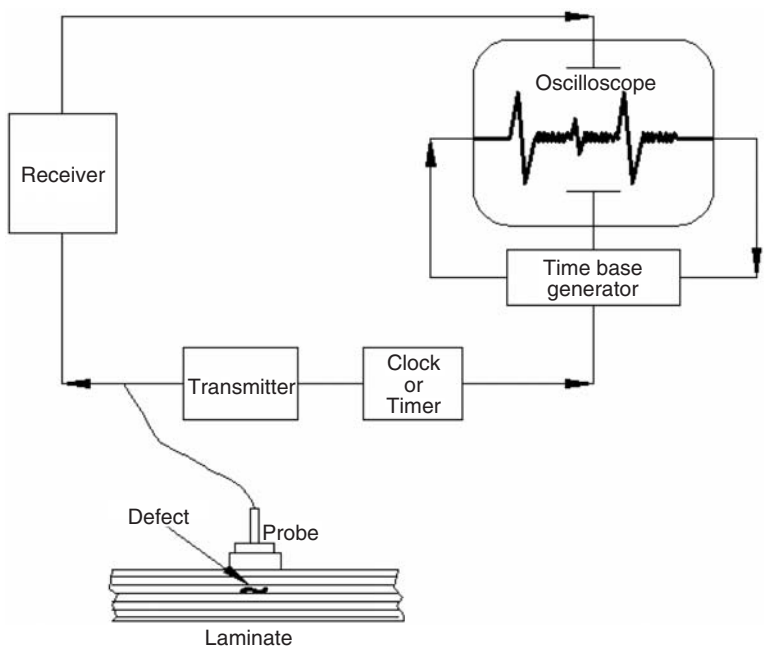

Figure 3. *Pulse-echo technique.*

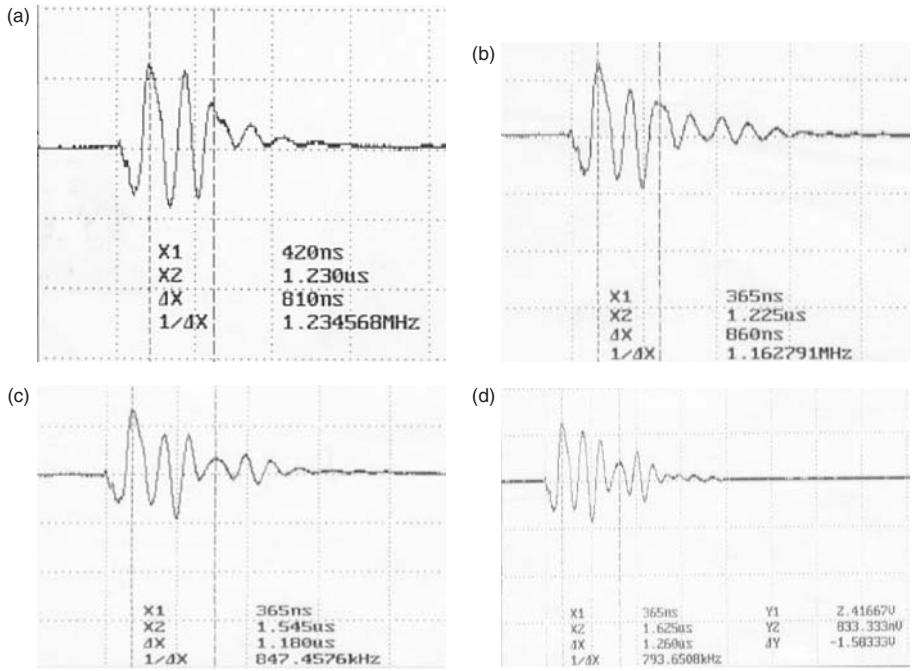

Figure 4. *Time of flight plots for constant defect size (Ø 8 mm) with varied location in an 8-layered laminate. (a) Defect located at midplane (below 4th layer) (b) Defect placed below 5th layer (c) Defect placed below 6th layer (d) Defect placed below 7th layer.*

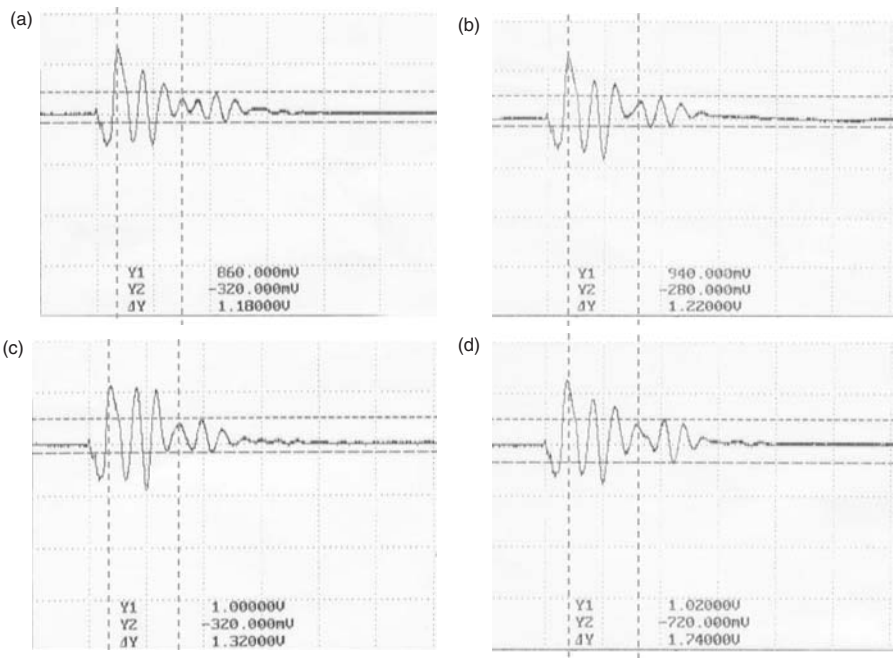

Figure 5. *Time of flight plots for constant defect size (Ø 6 mm) with varied location in an 8-layered laminate. (a) Defect located at midplane (below 4th layer) (b) Defect placed below 5th layer (c) Defect placed below 6th layer (d) Defect placed below 7th layer.*

From the scans and the table it is seen that while the time of flight is influenced only by the defect location (independent of size), the back wall echo amplitude varied with both the defect size and its location. In view of this, correlations were drawn between the time of flight and defect location and the back wall echo amplitude and defect size (diameter) as discussed below.

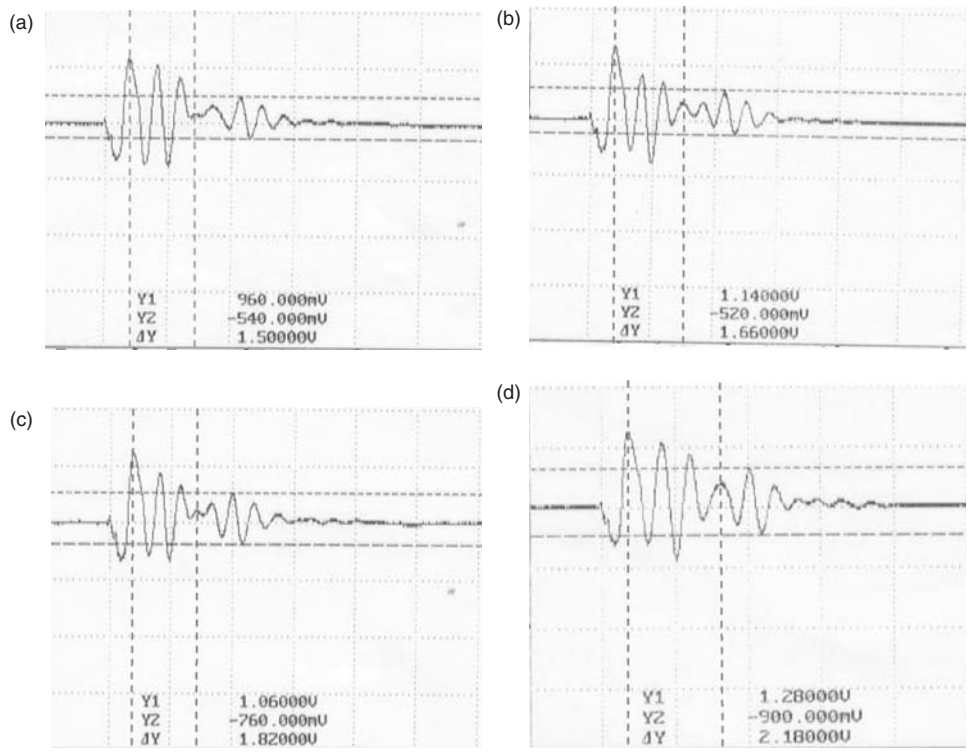

Figure 6. *Time of flight plots for constant defect size (Ø 4 mm) with varied location in an 8-layered laminate. (a) Defect placed below mid-plane (below 4th layer) (b) Defect placed below 5th layer (c) Defect placed below 6th layer (d) Defect placed below 7th layer.*

Table 1. Times of flight and back wall echo amplitudes for different defect locations and sizes.

Defect size	Ø 4 mm Defect size		Ø 6 mm Defect size		Ø 8 mm Defect size	
Location of defect	Time of flight (ns)	Back wall echo amplitude (mV)	Time of flight (ns)	Back wall echo amplitude (mV)	Time of flight (ns)	Back wall echo amplitude (mV)
Below 1st layer	Dead zone	—	Dead zone	—	Dead zone	—
Below 2nd layer	Dead zone	—	Dead zone	—	Dead zone	—
Below 3rd layer	Dead zone	—	Dead zone	—	Dead zone	—
Below 4th layer	800–820	1500	800–820	1180	800–820	980
Below 5th layer	860–880	1660	860–880	1240	860–880	1060
Below 6th layer	1160–1180	1820	1160–1180	1320	1160–1180	1220
Below 7th layer	1230–1270	2180	1230–1270	1700	1230–1270	1480
Below 8th layer	1430	2940	1430	2940	1430	2940

Time of Flight vs. Defect Location Correlations

Plot of the time of flight (Figure 7) from Table 1 shows that, as the defect location moves farther away from the probe, the flight time increases. The above curve can be represented by an equation of the form:

$$\theta = 16.43N^2 - 32.143N + 650.57. \quad (1)$$

Invariance of the Time of Flight with the Defect Size

Locally enlarged scans for the defects at four different locations and three diameters are presented in Figure 8.

From Figure 8, it can be seen that the time of flight is invariant with respect to the defect size at a given location, as presented in Table 1.

Back Wall Echo Amplitude vs Defect Size (Diameter) Correlations

Plot of the back wall amplitude values (Figure 9) from Table 1 shows that, the back wall echo amplitude decreases with increased defect size.

From Figure 8, it can be seen that, the back wall echo amplitude increases with increasing depth of location of defect for a given defect size, contrary to expectations, as presented in Table 1. The attenuation caused to the ultrasonic wave is proportional to the distance traversed by the wave after encountering the defect and hence the back wall echo amplitude increases as the defect is located closer to the back wall.

Destructive Test Results

Tables 2–7 show the compression, flexural and ILS strength data generated on a set of 5 specimens each.

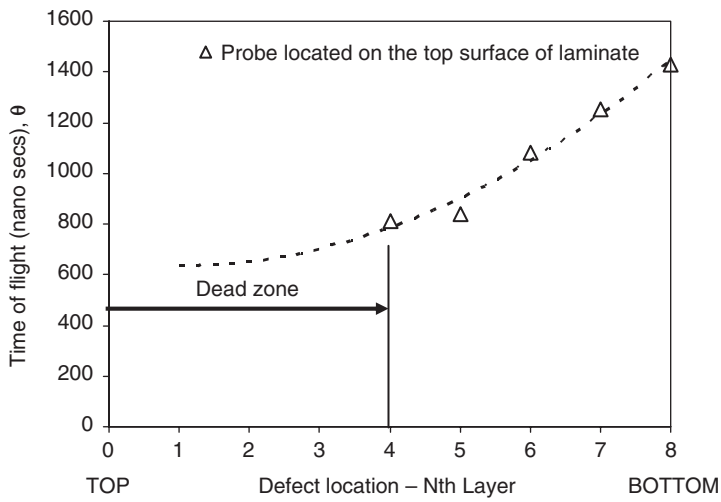

Figure 7. *Effect of depth of location of defect on time of flight.*

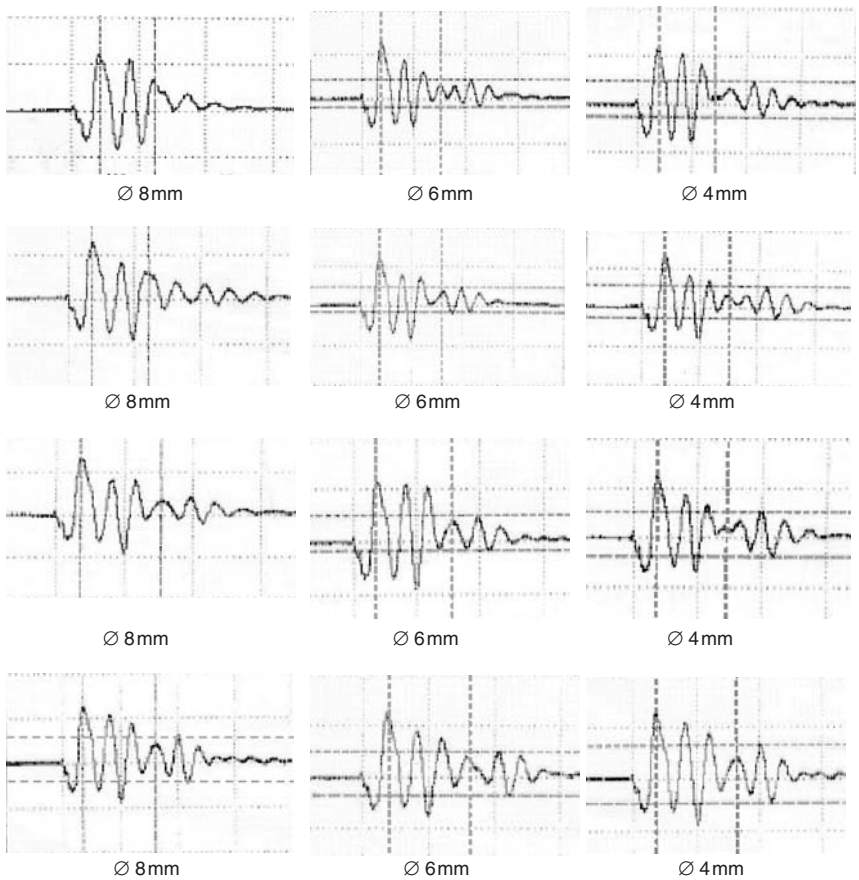

Figure 8. *(a)A-scans for defect placed at mid-plane. (b) A-scans for defect placed below 5th layer. (c) A-scans for defect placed below 6th layer. (d) A-scans for defect placed below 7th layer.*

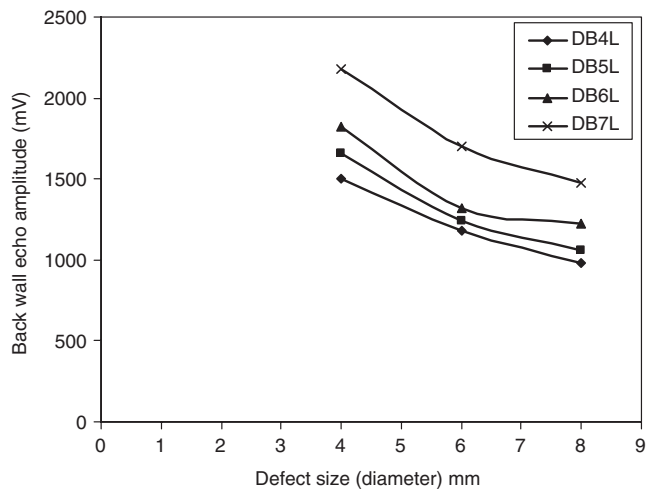

Figure 9. *Effect of defect diameter on back wall echo amplitude variance of the back wall echo amplitude with defect location.*

Table 2. Effect of location and size on the compression strength.

	Compression strengths (MPa)			
Location of defect	**Virgin Strength**	**Ø4**	**Ø6**	**Ø8**
Below 1st layer*	360	292.9	248.7	220.6
Below 4th layer	360	278.6	243.4	215.0
Below 7th layer*	360	292.9	248.7	220.6

Table 3. Percentage compression strength degradation.

	% Degradation of compression strength		
Location of defect	**Ø4**	**Ø6**	**Ø8**
Below 1st layer	18.63	30.91	38.72
Below 4th layer	22.61	32.38	40.27
Below 7th layer	18.63	30.91	38.72

Table 4. Effect of location and size on the flexural strength.

	Flexural strength (MPa)			
Location of defect	**Virgin strength**	**Ø4**	**Ø6**	**Ø8**
Below 1st layer	620	538.0	418.5	406.2
Below 4th layer (mid-plane)	620	565.7	519.6	476.4
Below 7th layer	620	562.0	484.0	465.7

Table 5. Percentage flexural strength degradation.

	% Degradation of flexural strength		
Location of defect	**Ø4**	**Ø6**	**Ø8**
Below 1st layer	13.22	32.5	34.48
Below 4th layer (at mid-plane)	8.75	16.19	23.16
Below 7th layer	9.35	21.9	24.88

Table 6. Effect of location and size on the ILSS.

	Interlaminar shear strength (kgf/mm^2)			
Location of defect	**Virgin strength**	**Ø4**	**Ø6**	**Ø8**
Below 1st layer	56.7	51.8	46.9	46
Below 4th layer	56.7	46.7	42.8	37.7
Below 7th layer	56.7	56	54.75	51.4

Compression Strength

From Tables 2 and 3, it can be seen that, the location of the defect (of a given diameter), does not affect the compression strength since loading is in the plane of the defect and the marginal variation (4%) is due to the failure mode that occurs due to the position of the defect whereas it is the defect size (diameter), which shows a more pronounced strength degradation effect on the composite (Figure 10).

The compression strength degradation when the defect is located below the 1st or the 7th layer should be identical (as signified by * in Table 2) and hence same values have been presented for both the cases in Tables 2 and 3. Further, it can be seen that the rate of strength degradation decreases with increasing defect diameter, which can be understood as the reduction of stress concentration factor with increasing ratio of hole diameter to the width of the plate as presented by Howland in [7] (Figure 11).

Flexural Strength

From the data (Tables 4 and 5), it can be observed that, the flexural strength is highest when the defect is located at mid-plane and is lowest when the defect is below the 1st layer

Table 7. Percentage ILSS degradation.

	% Degradation of flexural strength		
Location of defect	**Ø4**	**Ø6**	**Ø8**
Below 1st layer	8.6	17.27	18.94
Below 4th layer (at mid-plane)	16	24	33
Below 7th layer	1.27	3.42	9.33

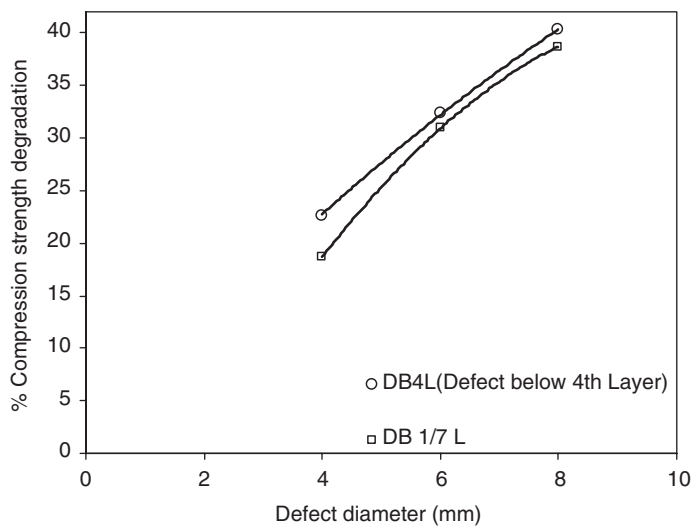

Figure 10. *Effect of defect size and location on the percentage compression strength degradation.*

(defect on compression side), while it is in the intermediate range when defect is below the 7th layer (defect on tension side) (Figure 12). The schematics (Figure 13) illustrating the method of (3-point bend) loading, clearly show that these results are very much in agreement with the theory on bending of beams.

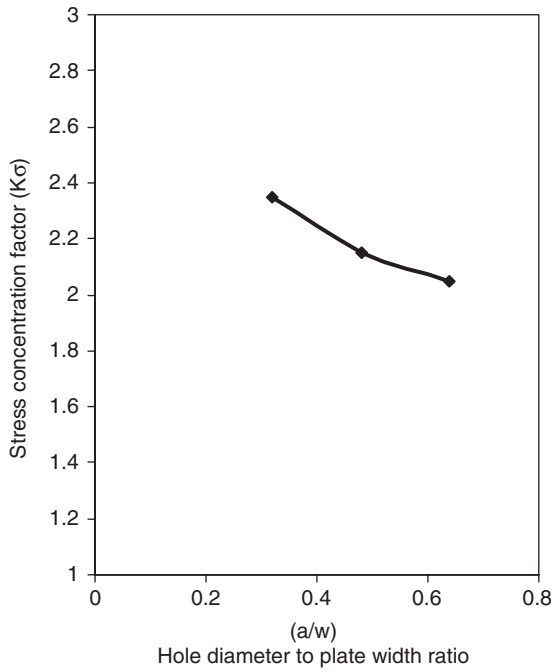

Figure 11. *Effect of ratio of hole diameter to plate width ratio on stress concentration factor [7].*

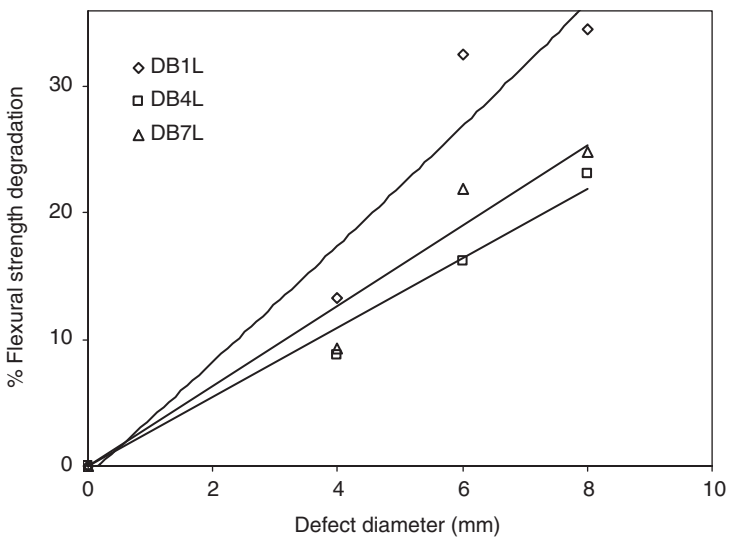

Figure 12. *Effect of defect size and location on the percentage flexural strength degradation.*

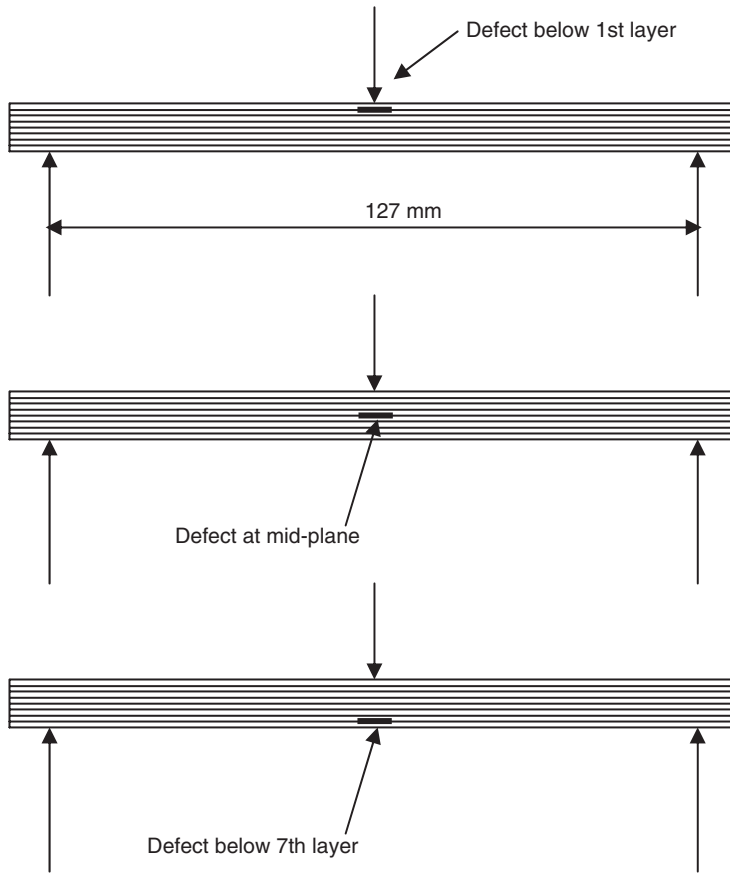

Figure 13. *Flexural (3-point bend) test loading arrangement.*

Interlaminar Shear Strength (ILSS)

Data from Tables 6 and 7 show that, the ILSS is lowest when the defect is located at mid-plane and is highest when the defect is below 7th layer (defect on tension side), while it is in the intermediate range when defect is below 1st layer (defect on compression side) (Figure 14). The schematics (Figure 15) illustrating the method of short-beam (3-point) loading, clearly shows that these results are very much in agreement with the short beam theory.

CORRELATION BETWEEN NON-DESTRUCTIVE CHARACTERIZATION PARAMATERS AND PROPERTY DEGRADATION

An attempt has been made to correlate the degradation in mechanical strength to the variation in the A-scan parameters viz. time of flight and back wall amplitude. It can be seen that, as the defect diameter increases, the back wall echo amplitude decreases, whereas, as the depth of defect location increases, the time of flight increases. The compression strength degrades with increasing defect diameter and increases

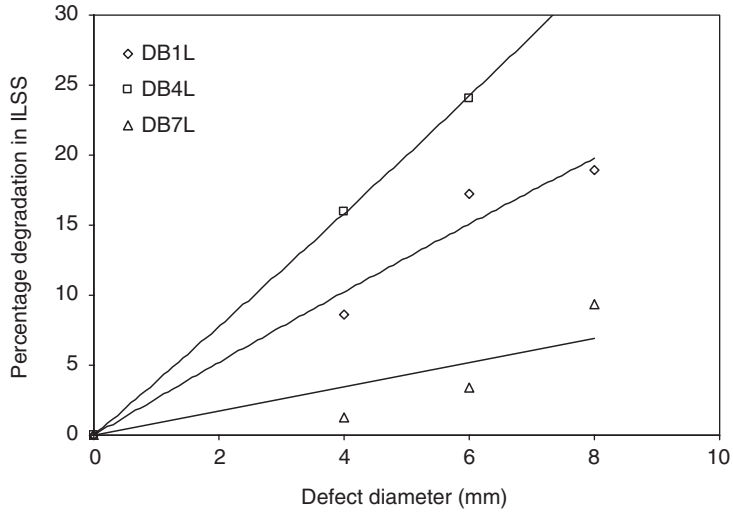

Figure 14. *Effect of defect size and location on the percentage interlaminar strength degradation.*

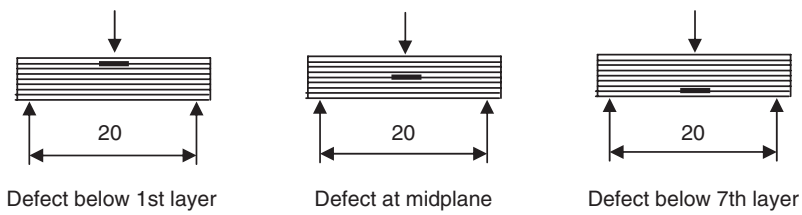

Figure 15. *Short beam (3-point bend) test loading arrangement.*

marginally with depth of location (from 4th to 7th layer). The flexural strength decreases with increasing defect diameter as well as with depth of location (from 4th to 7th layer). The ILSS decreases with increasing defect diameter, yet increases with depth of location (from 4th to 7th layer). Observing the variation of the mechanical property and the A-scan parameters with respect to each other, an empirical equation has been developed consisting of amplitude reduction ratio (A_2/A_1), time reduction ratio (T_1/T_2) and strength reduction ratio (S_2/S_1) terms that are related by a constant K. Tables 8, 9 and 10 contain the values of 'K_c', 'K_{fl}' and 'K_{sh}' for compression, flexural and interlaminar shear strengths of laminates with defects of different sizes and locations:

$$S_2 = K \times \sqrt{(A_2/A_1) \times (T_1/T_2)} \times S_1 \tag{2}$$

where
S_1 = virgin strength of the specimen (MPa)
S_2 = degraded strength of the specimen (MPa)
A_2 = back wall echo amplitude (mV) of defective laminate
A_1 = back wall echo amplitude (mV) of defect-free laminate
T_1 = time of flight (nano secs) for defect-free laminate
T_2 = time of flight (nano secs) for defective laminate

Table 8. Values of K_c for the compression strength correlation.

Diameter (mm)	Defect location: Mid-plane		Defect location: 7th Layer	
4	A_2/A_1	0.51	A_2/A_1	0.7414
	T_1/T_2	1.765	T_1/T_2	1.145
	S_2/S_1	0.7739	S_2/S_1	0.814
	K_c	**0.815**	K_c	**0.883**
6	A_2/A_1	0.40	A_2/A_1	0.5782
	T_1/T_2	1.765	T_1/T_2	1.145
	S_2/S_1	0.676	S_2/S_1	0.691
	K_c	**0.8032**	K_c	**0.8493**
8	A_2/A_1	0.3333	A_2/A_1	0.5034
	T_1/T_2	1.765	T_1/T_2	1.145
	S_2/S_1	0.5972	S_2/S_1	0.6128
	K_c	**0.7785**	K_c	**0.8075**

Table 9. Values of K_{fl} for the flexural strength correlation.

Diameter (mm)	Defect location: Mid-plane		Defect location: 7th Layer	
4	A_2/A_1	0.51	A_2/A_1	0.7414
	T_1/T_2	1.765	T_1/T_2	1.145
	S_2/S_1	0.9124	S_2/S_1	0.9064
	K_{fl}	**0.9613**	K_{fl}	**0.9842**
6	A_2/A_1	0.40	A_2/A_1	0.5782
	T_1/T_2	1.765	T_1/T_2	1.145
	S_2/S_1	0.838	S_2/S_1	0.78
	K_{fl}	**0.9956**	K_{fl}	**0.96**
8	A_2/A_1	0.3333	A_2/A_1	0.5034
	T_1/T_2	1.765	T_1/T_2	1.145
	S_2/S_1	0.7684	S_2/S_1	0.7511
	K_{fl}	**1.0**	K_{fl}	**0.99**

Table 10. Values of K_{sh} for the ILSS correlation.

Diameter (mm)	Defect location: Mid-plane		Defect location: 7th Layer	
4	A_2/A_1	0.51	A_2/A_1	0.7414
	T_1/T_2	1.765	T_1/T_2	1.145
	S_2/S_1	0.824	S_2/S_1	0.988
	K_{sh}	**0.87**	K_{sh}	**1.07**
6	A_2/A_1	0.40	A_2/A_1	0.5782
	T_1/T_2	1.765	T_1/T_2	1.145
	S_2/S_1	0.756	S_2/S_1	0.966
	K_{sh}	**0.898**	K_{sh}	**1.19**
8	A_2/A_1	0.3333	A_2/A_1	0.5034
	T_1/T_2	1.765	T_1/T_2	1.145
	S_2/S_1	0.665	S_2/S_1	0.91
	K_{sh}	**0.87**	K_{sh}	**1.2**

The average values of K_c, K_{fl} and K_{sh} were assumed as 0.8, 1.0 and 0.88 respectively (from data in Tables 8–10) and the reduced strengths were recalculated and compared with the experimental values.

From the correlation curves between the experimental compression, flexural and ILS strengths and those predicted by the empirical equation, it can be seen that the correlations are very good for the case of defect placed at the mid-plane (Figures 16–18). However, for the case of defect below 7th layer, as compared to the compression and flexural strengths (Figures 19 and 20), larger deviations are seen for the ILSS case (Figure 21). This is because of the variation in the mean K_{sh} values obtained for the mid-plane and the 7th layer case (Table 10).

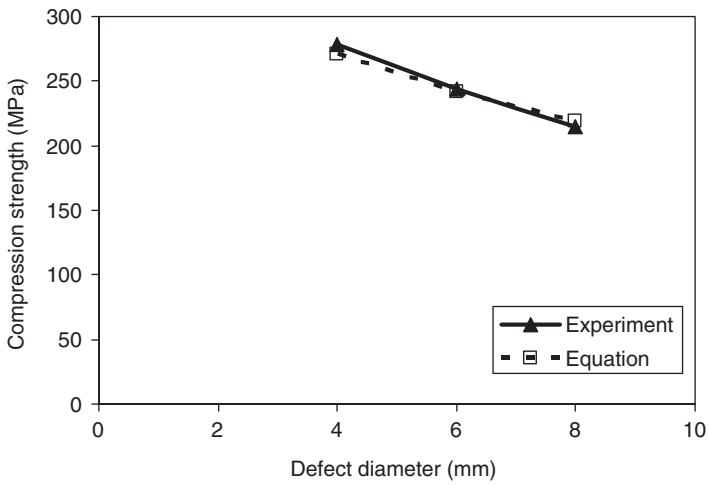

Figure 16. *Compression strength correlation when defect is at mid-plane.*

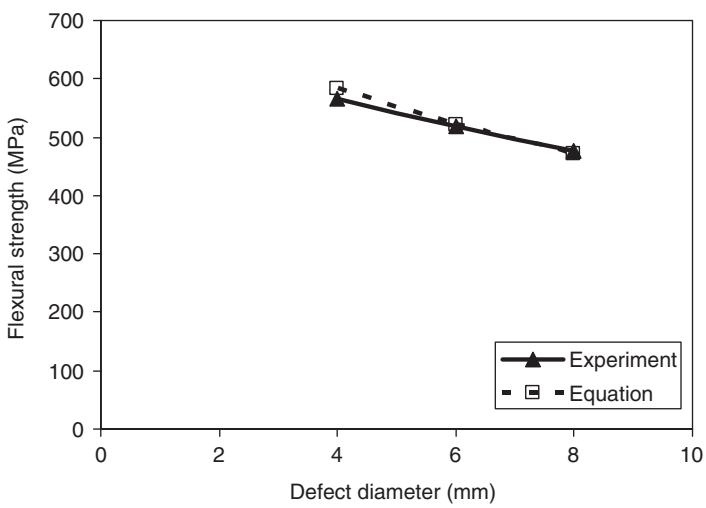

Figure 17. *Flexural strength correlation when defect is at mid-plane.*

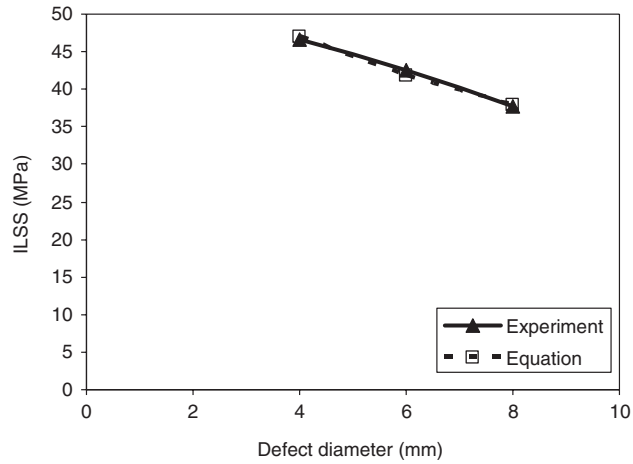

Figure 18. *ILSS correlation when defect is at mid-plane.*

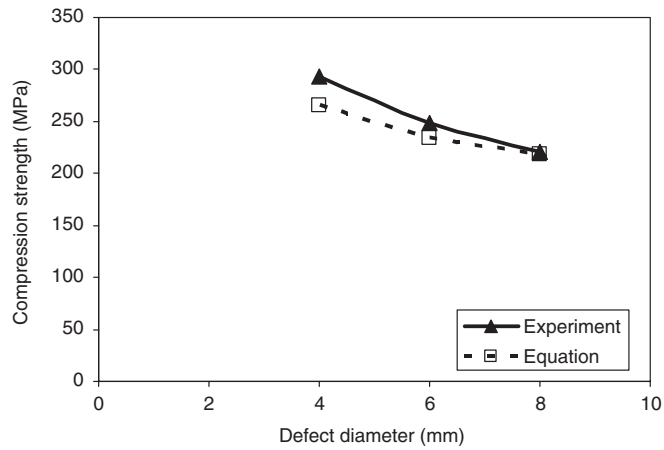

Figure 19. *Compression strength correlation when defect is below 7th layer.*

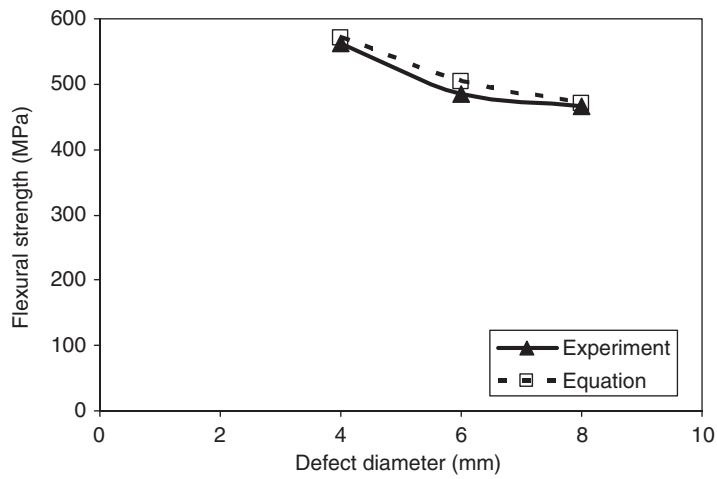

Figure 20. *Flexural strength correlation when defect is below 7th layer.*

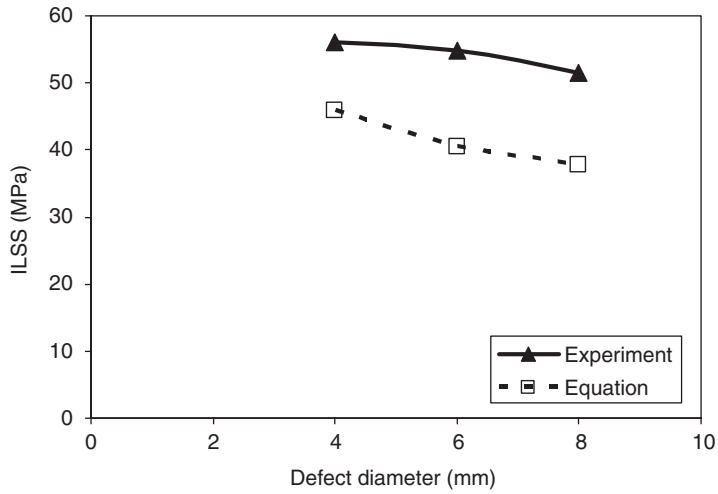

Figure 21. *ILSS correlation when defect is below 7th layer.*

CONCLUSION

An attempt was made to correlate the time of flight and back wall echo amplitude (NDT parameters) and strength degradation (obtained through destructive tests) of glass/epoxy composites by an empirical equation, for different defect sizes and locations. It was found that the defect location could be identified by the time of flight parameter, and it was found that it increased as the defect moved away from the probe and was independent of the defect size. The defect size could be characterized by the back wall echo amplitude. It was observed that the back wall echo amplitude decreased with increased defect size, indicating attenuation of the sound energy; however, the amplitudes increased as the defect moved nearer to the back wall because of the reduction in the distance traveled by the attenuated wave.

Good correlations were seen between the composite strength degradation measured from the destructive tests and those predicted using the empirical equation, with NDT parameters (time of flight and back wall echo amplitude) and virgin strength of the composite as inputs.

ACKNOWLEDGEMENTS

The authors are thankful to Dr. A. R. Upadhya, Director, National Aerospace Laboratories, Bangalore, for the encouragement received and they further acknowledge the help rendered by Sri. M. Rajendra Prakash, in specimen testing.

REFERENCES

1. Miller, A. G., Lovell, D. T. and Seferic, J. C. (1994). The Evolution of an Aerospace Material: Influence of Design, Manufacturing and In-service Performance *Composite Structures*, **27**(1–2): 193–206.
2. Posakony, G. J. (1986). Experimental Analysis of Ultrasonic Responses from Artificial Defects, *Materials Evaluation*, **44**(13): 1567–1572.

3. Severin, F, Maeva, E, Ptchelintsev, A. and Maev, R. (2001). The Acoustical Monitoring of Internal Delaminations in Fibre Reinforced Composites. Review of Progress in Quantitative Non Destructive Evaluation, Edited by Thomson, D. O. and Chimenti, D. E., *American Institute of Physics*, **20**: 419–432.
4. Wooh, S. C. and Wei, C. (1999). A High-fidelity Ultrasonic Pulse-echo Scheme for Detecting Delaminations in Composite Laminates, *Composites*, **30B**(5): 433–441.
5. Bar-Cohen, Y., Arnon, U. and Meron, M. (1979). Ultrasonic Non Destructive Evaluation and Method for the Detection and Identification of Defects in Filament Wound Glass Fiber – Reinforced Plastic Tubes, *Materials Evaluation*, **37**(8): 51–55.
6. Judd, N. C .W. and Wright, W. W. (1978). Voids and their Effect on the Mechanical Properties of Composites – An Appraisal, *SAMPE Journal*, **14**(1): 10–14.
7. Lingaiah, K. (1986). *Machine Design Data Handbook*, Vol. 1, Chapter IV, pp. 52–70, **2nd Edn** (Reprint), Suma Publishers, Bangalore, India.